Experimental Validation of Underwater Depth and Orientation Control Using Reversible Fuel Cell Electrolysis

Denizcan Koc[1], Qiang Zhu[1], Fathi Ghorbel[2], Zheng Chen[1*]

***Abstract*—In this paper, we present the experimental validation of our previous research on buoyancy control devices (BCDs) that are based on proton exchange membrane (PEM) electrolysis. These devices are used to control the buoyancy and orientation of autonomous underwater vehicles (AUVs) by volume adjustments of the output gases (hydrogen and oxygen) from PEM electrolysis. Two different devices are designed. Using the first device, we performed experiments to demonstrate the effectiveness of using regular (hard) thrusters and (soft) PEM electrolysis for depth control. We utilized a Model Predictive Control (MPC) law for this purpose. The experimental results showed that the addition of the soft actuator brings a significant amount of energy savings. Furthermore, we designed a second device to validate the simultaneous control of the depth and orientation of BCDs that use only PEM electrolysis. Two different closed-loop controllers are designed to use two PEM electrolyzers. The experimental results demonstrated their ability to control both vertical movement and orientation simultaneously. A feasibility study on deep ocean application has been conducted and simulation results have shown that an industrial PEM based BCD can save up to 90% of energy when an underwater vehicle operates a payload of 5 kg under 300 bar water pressure.**

I. INTRODUCTION

Numerous underwater robotic devices, including remotely operated vehicles (ROVs) and autonomous underwater vehicles (AUVs), are extensively used in the oil and gas industry for various purposes, such as offshore drilling [1]. However, one of the significant issues with underwater robotics is the sudden change in buoyancy, especially for devices that change their overall weight due to the grabbing or releasing of items underwater [2]. Underwater robots may often need to adjust their buoyancy when dealing with applications such as investigating the impact of the Deepwater Horizon explosion on historic shipwreck-associated sediment microbiomes, which require the capture or release of materials [3].

Using Direct Current (DC) propellers for vertical movement is a common way to control the depth of underwater vehicles [4]. DC motors are preferred because they can provide a lot of power even when the vehicle is heavy, weighing several tons [5]. However, there are some disadvantages to using DC propellers for depth control, such as high energy consumption and noise generation [6]. When the total mass of the vehicle changes, the weight will no longer be equal to the buoyancy force. As a result, the propellers will need to run continuously, which is why some researchers are exploring alternative solutions based on adjustable buoyancy rather than relying on the propellers to constantly apply an external force.

A common way to adjust the buoyancy of a device is by pumping or sucking water to increase or decrease its weight until it reaches a neutral buoyancy level [7]. However, this method requires a lot of power to release the water when the pressure difference between the environment and the water tank is significant. This becomes a major challenge in deep-ocean applications, where the depth can reach thousands of meters [8]. Another method of controlling buoyancy is to use compressed air and release it when needed [9]. However, this method has some drawbacks, such as limited air supply, excessive heat generation, and high friction drag that can affect the buoys [10], [11]. PEM electrolysis offers several advantages over previous gas generation and compressed air methods for buoyancy control. These include precise control with finer increments in gas generation, eliminating the need for high-risk pressure tanks required in compressed air systems [12], [13], reduced maintenance due to fewer moving parts, and the dual functionality of energy storage when operating in the fuel cell model [14].

Our research group has been studying an innovative way to achieve adjustable buoyancy for underwater ROVs using PEM electrolyzers. PEM electrolysis is a chemical reaction that uses electrical energy to convert water into hydrogen and oxygen gas in a cell containing a solid polymer electrolyte membrane that selectively conducts protons, allowing hydrogen ions to pass through while blocking electrons [15]. We used the hydrogen and oxygen gases produced through this process to fill the ROV balloons, thus increasing their total volume and adjusting their buoyancy [16]–[18]. Our extensive exploration of this approach has shown that traditional thrusters can be used for coarse motion, while fine motion is achieved by electrolysis [19]–[22]. The simulation results have shown significant energy savings [19], [20] and that this approach can result in substantial energy savings compared to using traditional thrusters alone [23]. Recently, we conducted further studies [24], [25] that extended our previous results and validated that buoyancy control devices based on PEM electrolysis can be used exclusively for buoyancy and orientation control.

This paper is an extension of our previous research [19]–[25] and focuses on experimental validation. The major contributions of this study can be listed as follows:

1) A comprehensive physics-based model of the hybrid system, integrating thrusters and PEM electrolysis, has been developed. An MPC is designed on the basis of this model and is experimentally validated, demonstrating its effectiveness.

2) The addition of PEM electrolysis to conventional thrusters is analyzed in terms of energy consumption, with

*Corresponding author: Zheng Chen, Email: zchen43@central.uh.edu.

[1]Denizcan Koc and Qiang Zhu are Ph.D. students in the Mechanical Engineering Department, University of Houston, 4800 Calhoun Rd, Houston, TX 77004. dkoc3@uh.edu (DK), qzhu11@uh.edu (QZ).

[2]Dr. Fathi Ghorbel is a Professor of Mechanical Engineering, Rice University, 6100 Main St, Houston, TX 77005. ghorbel@rice.edu.

[1]Dr. Zheng Chen is an Associate Professor of Mechanical Engineering, University of Houston, 4800 Calhoun Rd, Houston, TX 77004. zchen43@central.uh.edu.

a direct comparison of control inputs, providing quantifiable insights into the efficiency improvements introduced by this approach.

3) A second device has been designed to allow actuation in multiple directions (both depth and orientation). The physics-based model and controllers are developed. In this study, experimental validation of this multidirectional actuation using PEM electrolysis is presented for the first time.

The remainder of the paper is structured as follows. Section II provides an overview of the dynamic model of the buoyancy-enabled depth control device, and explains the theoretical modeling of the maneuvering and depth control device. The control methods used in those devices and the simulation results are elaborated in Section III together with the identification of the system parameters that will be used in simulations. After presenting the control methods and simulation results, the experimental setup and results are discussed in Section IV. Section V presents a comprehensive feasibility study for real-time applications of the proposed method. Finally, the paper concludes with an overall conclusion and possible future work in Section VI.

II. Modeling of the Buoyancy-enabled Depth and Orientation Control Device

In this section, a model of the buoyancy-enabled depth and orientation control device will be provided. First, we will present a device with both thrusters and PEM electrolzyers for vertical motion control only. Second, we will derive a physics-based model of this device. Lastly, we will present a 2-dimensional (2D) maneuverable device with both depth and orientation control and derive a model for it.

A. Device Description

The device is composed of a chamber that houses all the electronics, two DC motors attached to the chamber, and two balloons that store hydrogen and oxygen gases, respectively. The prototype of the device can be found in Fig. 1. A model of the device is needed for the predictive control design of the model. Fig. 2 illustrates the schematic and free-body diagram of the underwater device. The constant volume of the device is represented as V_0, and the variable volume of the balloons is represented as V_b. The x represents the vertical position of the device. The positive direction is from the bottom of the aquarium to the surface of the water.

B. Modeling of the Vertical Motion Dynamics

There are four significant forces acting on the device. Two are in the positive direction, which is the thrust force and the buoyancy force, and two are in the negative direction, which are the drag force and the weight of the device. The minor effects on the device dynamics caused by environmental disturbances are neglected. The thrust force is represented by $F_t(t)$, which is the force introduced by the DC propellers. The buoyancy force is represented by $F_b(t)$. The drag force is represented by $F_d(t)$, which can be considered as a friction force caused by the interaction between the fluid and the

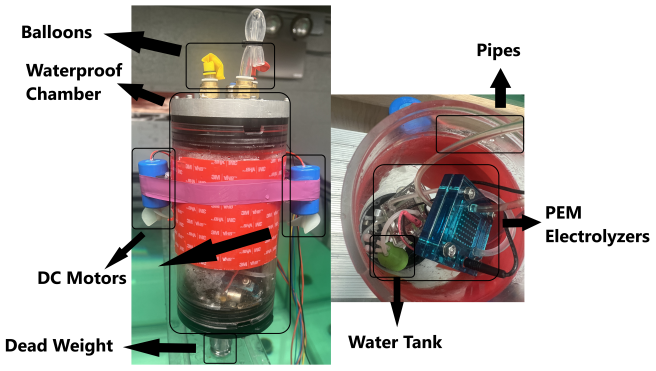

Fig. 1. Prototype of the device with depth control only.

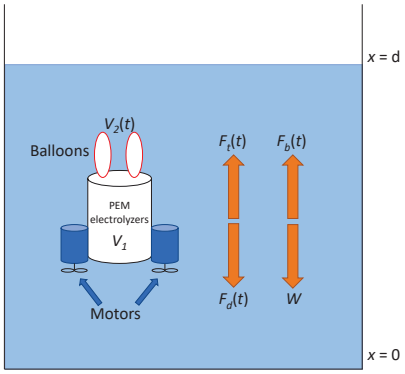

Fig. 2. Schematic of vertical motion dynamics.

device during the motion. The weight is represented as W.

By including all four forces, the equation of motion by using the force equilibrium in the vertical direction is given by

$$F_{net} = -W + F_b(t) + F_t - F_d(t). \tag{1}$$

The weight and drag forces are given as

$$W = mg, \tag{2}$$

$$F_d(t) = b\dot{x}(t), \tag{3}$$

where m is the mass, g is the gravitational acceleration, b is the drag coefficient, and $x(t)$ is the variable depth where the upward direction is assumed as positive direction of the depth. Therefore, $\dot{x}(t)$ is the velocity of the device in vertical direction.

The buoyancy force is related to the density of the fluid and the total volume of the device by

$$F_b(t) = \rho(V_0 + V_b(t))g, \tag{4}$$

where ρ is the density of the fluid and $V_b(t)$ is the total volume of the balloons. $V_b(t)$ is expressed in terms of the initial volume of the balloons. The volume of the generated gas is expressed by using Boyle's law as

$$V_b(t) = \frac{P_{atm}}{P_{atm} + \rho g(d - x(t))} \cdot (V_{in} + V_e(t)), \tag{5}$$

where d represents the total depth of the aquarium, V_{in} represents the initial volume of the balloons measured at the surface, P_{atm} represents the atmospheric pressure and $V_e(t)$ represents the volume of the gas generated. The gas generation rate can be related to the current input to the water electrolyzers by using Faraday's first law of electrolysis [21] as

$$\dot{V}_e(t) = (\frac{I(t)}{2F} \cdot V_m) \cdot N_{cell} \cdot \frac{3}{2}, \tag{6}$$

where $I(t)$ is the current input, F is the Faraday constant, V_m is the molar volume of ideal gas, and N_{cell} is the number of electrolyzers used in the application. Since the current input is the only time-varying variable, it can be integrated as

$$V_e(t) = (\frac{\int I(t)dt}{2F} \cdot V_m) \cdot N_{cell} \cdot \frac{3}{2}. \tag{7}$$

It is preferred to control the voltage input instead of the current in our experiments due to the usage of the Dspace controller desk (DS1104, dSPACE Inc.), which manipulates the input voltage. Therefore, the voltage-current relation of PEM electrolyzers can be obtained by a system identification process. The linear relation is expected to be obtained for a limited range of voltage input [26]. The formulation can be expressed as

$$I(t) = K_1 \upsilon_{in,PEM}(t) + K_2 \quad \text{for} \quad 2 \text{ V} \leq \upsilon_{in,PEM}(t), \tag{8}$$

where $\upsilon_{in,PEM}(t)$ represents the voltage input to the PEM electrolyzers, and K_1 and K_2 are the coefficients which can be identified by a experimental validation.

The thrust force of DC motors in terms of voltage input is expected to follow a quadratic profile [27]. The formulation can be expressed as

$$F_t(t) = K_3 \upsilon_{in,DC}^2(t) + K_4 \upsilon_{in,DC}(t) + K_5 \quad \text{for} \quad 0.7 \text{ V} \leq \|\upsilon_{in,DC}(t)\|, \tag{9}$$

where $\upsilon_{in,DC}(t)$ represents the voltage input to the DC motors and K_3, K_4, K_5 are the coefficients which will be carried out in the system identification part.

The coefficients are specified in Table I. Using the expressions in Eqs. 2-9, Eq. 1 becomes

$$m\ddot{x} = -mg + \rho(V_0 + \frac{P_{atm}}{P_{atm} + \rho g(d - x(t))} \cdot (V_{in} + ((\frac{\int K_1 \upsilon_{in,PEM}(t) + K_2 dt}{2F} \cdot V_m) \cdot N_{cell} \cdot \frac{3}{2}))) g + K_3 \upsilon_{in,DC}(t)^2 + K_4 \upsilon_{in,DC}(t) + K_5 - b\dot{x}(t). \tag{10}$$

Combining Eq. 7 and Eq. 10, the state space representation of the equation of motion is given by

$$\begin{bmatrix} \dot{X}_1 \\ \dot{X}_2 \\ \dot{X}_3 \end{bmatrix} = \begin{bmatrix} X_2 \\ -g + (V_0 + \frac{P_{atm}}{P_{atm} + \rho g(d - X_1)} \cdot V_{in}) \frac{\rho g}{m} \\ \frac{K_1 u_2 + K_2}{2F} \cdot V_m \cdot N_{cell} \cdot \frac{3}{2} \end{bmatrix} + \begin{bmatrix} 0 \\ (\frac{P_{atm}}{P_{atm} + \rho g(d - X_1)}) X_3 \frac{\rho g}{m} + \frac{K_3 u_1^2 + K_4 u_1 + K_5}{m} - \frac{bX_2}{m} \\ 0 \end{bmatrix}, \tag{11}$$

where the state vector and control vector are given by:

$$\begin{bmatrix} X_1 \\ X_2 \\ X_3 \end{bmatrix} = \begin{bmatrix} x(t) \\ \dot{x}(t) \\ V_e(t) \end{bmatrix}, \begin{bmatrix} u_1 \\ u_2 \end{bmatrix} = \begin{bmatrix} \upsilon_{in,DC}(t) \\ \upsilon_{in,PEM}(t) \end{bmatrix}. \tag{12}$$

C. Modeling of the Rotational Motion Dynamics

Previous studies on PEM electrolysis-based buoyancy control focused on one-dimensional motion in the vertical direction. In this study, another device has been developed to provide soft actuation by PEM electrolyzers in the angular direction in addition to the vertical direction. The design is made by attaching two buoyancy control devices (BCDs) and creating a single rigid body out of two BCDs, as shown in Fig. 3. The schematic for device modeling can be found in Fig. 4.

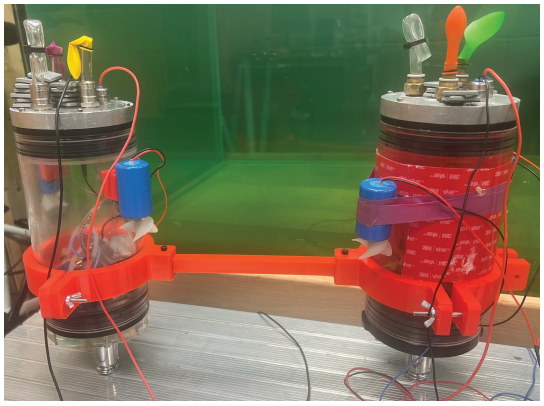

Fig. 3. Prototype of the device with both depth and orientation control.

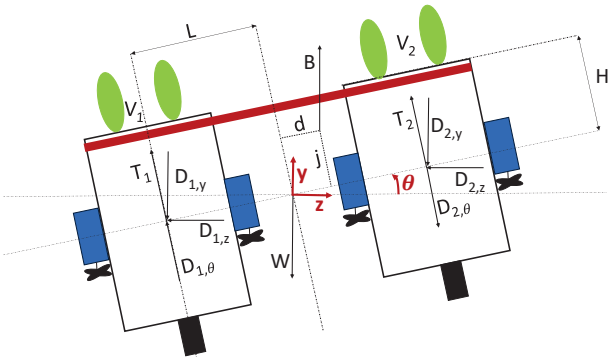

Fig. 4. Schematic of the rotational motion dynamics.

The forces acting on the device are the thrust forces generated by the DC motors (T_1 and T_2), the drag forces as resistance to movement in horizontal, vertical and rotational directions (D_x, D_y and D_θ), the buoyancy force of the overall device (B), and the weight of the overall device (W). The weight and drag

forces are given by

$$W = Mg, \tag{13}$$

$$D_{1,y} + D_{2,y} = c_y \dot{y}(t), \tag{14}$$

$$D_{1,z} + D_{2,z} = c_z \dot{z}(t), \tag{15}$$

$$D_{1,\theta} + D_{2,\theta} = c_\theta \dot{\theta}(t), \tag{16}$$

where M represents the total mass of the device in Fig. 4, c_y, c_z, and c_θ represent the damping coefficients in the horizontal, vertical and rotational directions, respectively. The assumption is to have homogeneous damping forces in both BCDs because of the device symmetry. The rotation of the device without the help of thrusters can only be caused by the difference in the center point of buoyancy force and weight. Although the center point of the weight is the center of mass, the center of buoyancy is actually the center of volume. Therefore, asymmetric volume distribution while having symmetric mass distribution will cause a difference in center points. Using Newton's second law, the overall dynamics of the device shown in Fig. 4 is given by

$$-T_1 \sin(\theta) - T_2 \sin(\theta) - c_z \dot{z} = M\ddot{z}, \tag{17}$$

$$T_1 \cos(\theta) + T_2 \cos(\theta) - c_y \dot{y} + \rho g(V_0 + V_1 + V_2) - Mg = M\ddot{y}, \tag{18}$$

$$-T_1 L + T_2 L - c_\theta \dot{\theta} + \rho g(V_0 + V_1 + V_2)(\cos(\theta) d - \sin(\theta) j) = I\ddot{\theta}, \tag{19}$$

where variables z, y, and θ represent the position on the horizontal axis, the vertical axis, and the orientation with respect to the positive z axis, respectively. V_1 is the volume of balloons attached to the first BCD, and V_2 is the volume of balloons attached to the second BCD. The expressions for d and j are given by

$$d = \frac{V_2 L - V_1 L}{V_0 + V_1 + V_2}, \tag{20}$$

$$j = \frac{V_2 H + V_1 H}{V_0 + V_1 + V_2}, \tag{21}$$

where the lengths L and H are shown in Fig. 4.

D. System Identification

The system identification was conducted to identify the coefficients in Eqs. 7-8. The first experiment was performed for PEM electrolyzers by applying voltages in a range from 2V to 9V and observing the behavior of current output in steady state. The profile can be observed in Fig. 5. Another experiment has been performed by applying a thrust force to the device and bringing it to a steady state. Since the weight and initial volume of the device are known, and acceleration is zero at steady state, Newton's second law will directly give the thrust force by subtracting the buoyancy force from the weight. The profile can be observed in Fig. 6.

Although the relation between voltage input to the gas generation rate and the thrust force is explored, it should be noted that the actuator dynamics might vary this relationship. The performance of the DC motor can alter due to hydrodynamic effects and possible corrosion. Moreover, the performance of the PEM electrolyzer is also not stationary as a result of the degradation of the membrane or electrode. The results of Figs. 5 and 6 are used as approximations for their dynamics that will be used to design the controller.

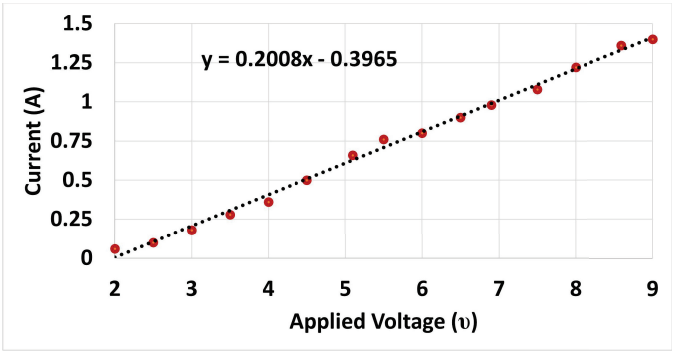

Fig. 5. Applied voltage vs current of PEM Electrolyzers

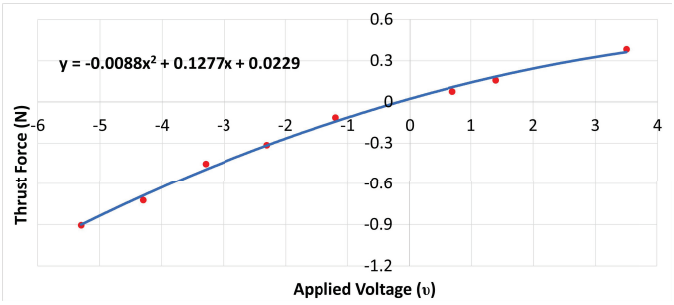

Fig. 6. Applied voltage vs thrust force of the thrusters.

TABLE I
IDENTIFIED PARAMETERS

Parameter	Value	Unit
F	96485	C/mol
V_m	24789	ml/mol
b	0.04	Ns/m
d	1000	mm
g	9.81	m/s^2
K_1	0.2008	
K_2	-0.3965	
K_3	-0.0088	
K_4	0.1277	
K_5	0.0229	
m	2643	g
N_{cell}	2	
P_{atm}	101325	Pa
ρ	997	kg/m^3
V_{in}	0	m^3
V_1	$2.621 \cdot 10^{-3}$	m^3
k	$1/(2.5803 \cdot 10^{-8})$	
c_y	0.3	Ns/m
I	0.1646	$kg \cdot m^2$
L	0.16	m
H	0.16	m
c_θ	0.3	Ns/rad
V_0	0.0053	m^3

III. CONTROL SYSTEM DESIGN AND SIMULATION

The overall closed-loop control system of the vertical motion control device is provided in Fig. 7. The tracking error goes through two controllers, which are for the DC motors

and the PEM electrolysis. The pressure sensor depth signal is used as feedback in the control loop, which creates an MISO system.

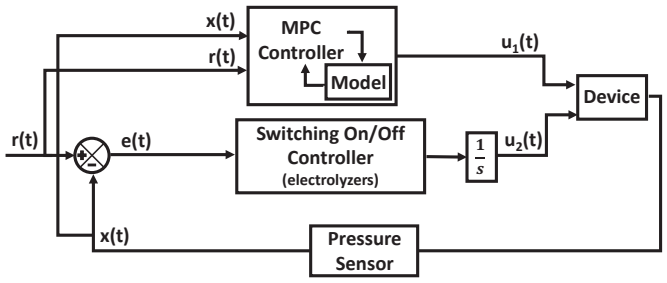

Fig. 7. Schematic of the control loop.

A. Control of the Thrusters

Model Predictive Control (MPC) is chosen as the controller of the thrusters. Since the thrusters are likely to consume more energy compared to the PEM electrolysis, as well as being more significant in transient response, the MPC is selected so that the optimal control performance of the MPC can provide more energy-efficient performance compared to the traditional controllers and having a more precise depth tracking by predicting the future steps from the model of the dynamics of the device. MPC is a control method that minimizes a linear quadratic cost function based on the device dynamics model [28] [29]. The MPC algorithm predicts the future states $(y_k, y_{k+1}, ..., y_{k+P-1})$ based on the input of the current state for a limited time interval, which is called the prediction horizon (P), and choosing the set of controllers $(u_k, u_{k+1}, ..., u_{k+M-1})$ for a finite time interval, which is called the control horizon (M). The controllers are selected so that they can minimize the cost function for the defined prediction horizon [30] [31]. After the set of controllers is determined, the first element (u_0) is sent as a control input to the device. This algorithm is repeated for each control loop during a simulation or real experiment [32] [33].

The performance index of the MPC can be expressed as the following linear quadratic term:

$$J(t) = \int (Q(x(t) - r(t))^2 + Ru_1^2(t))dt, \tag{22}$$

where Q represents the cost of the state, and R is the cost of the DC motor controller under conditions $Q \succeq 0$ and $R \succ 0$. The MPC is designed by linearizing the dynamics of hard actuators by assuming that the input from soft actuation is the disturbance of the system. The new state-space representation without the dynamics of the PEM electrolysis is given by

$$\begin{bmatrix} \dot{X}_1 \\ \dot{X}_2 \end{bmatrix} = \begin{bmatrix} X_2 \\ -g + V_1 \frac{\rho g}{m} + \frac{K_3 u_1^2 + K_4 u_1 + K_5}{m} - \frac{bX_2}{m} \end{bmatrix}. \tag{23}$$

Linearization is conducted around an equilibrium point. The equilibrium point of this state space equation is $(X_1^*, 0)$ where X_1^* is a free parameter. This is expected because the device can be stabilized at any desired depth. The control input is zero at the steady state when the device becomes neutrally buoyant, which will be the case in the real experiment when the PEM electrolysis provides the necessary change in volume. Jacobian linearization method is applied to linearize this state-space equation by classifying the terms as

$$\begin{bmatrix} \dot{X}_1 \\ \dot{X}_2 \end{bmatrix} = J(X) \begin{bmatrix} X_1 - X_1^* \\ X_2 - X_2^* \end{bmatrix} + J(U) \begin{bmatrix} U_1 - U_1^* \\ U_2 - U_2^* \end{bmatrix}, \tag{24}$$

where $J(X)$ and $J(U)$ are Jacobian matrices for input of the state and control. When Jacobian matrices are determined by taking the derivatives for the corresponding variables [34], Eq. 24 is rewritten by

$$\begin{bmatrix} \dot{X}_1 \\ \dot{X}_2 \end{bmatrix} = \begin{bmatrix} 0 & 1 \\ 0 & \frac{-b}{m} \end{bmatrix} \begin{bmatrix} X_1 - X_1^* \\ X_2 - X_2^* \end{bmatrix} + \begin{bmatrix} 0 & 0 \\ \frac{K_4}{m} & 0 \end{bmatrix} \begin{bmatrix} U_1 - U_1^* \\ U_2 - U_2^* \end{bmatrix}. \tag{25}$$

Using the parameters in Table I, the linearized state-space equation becomes

$$\dot{x} = \begin{bmatrix} 0 & 1 \\ 0 & -0.0151 \end{bmatrix} x + \begin{bmatrix} 0 \\ 0.0483 \end{bmatrix} u,$$
$$y = \begin{bmatrix} 1 & 0 \end{bmatrix} x. \tag{26}$$

This linearized model is used in Matlab Simulink to design a predictive controller model. The parameters for MPC are determined by running simulations of the nonlinear model by using the designed MPC and observing the response. The selected values of the parameters can be found in Table II. The simulation result using this MPC block, including all the dynamics of the device (as in Eq. 11) can be found in Fig. 8. The MPC takes the input and minimizes the cost function (Eq. 22) by using the linearized state-space equation (Eq. 26).

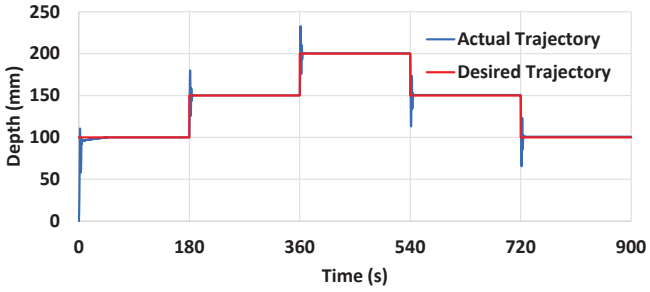

Fig. 8. The simulation result of depth tracking using MPC.

B. Control of the PEM Electrolyzers

The PEM electrolysis controller is designed to track the error signal in a way that runs with maximum performance when an increase in the neutral buoyancy is needed, is turned off when the volume is already at the desired level, and runs at maximum performance in reversible mode when a decrease in the neutral buoyancy is needed. In that way, the PEM electrolysis adjusts the volume of the device until it becomes neutrally buoyant.

C. Orientation Control Design

The orientation control is carried out by the PEM electrolyzers only without using any thrusters to validate that pure PEM electrolysis can be used for actuation in vertical and angular

directions simultaneously. Therefore, the thrust forces of the DC motors (T_1 and T_2 in Eqs. 17-19) are taken as zero in the equation of motion of the device. The controllers are voltage inputs to the PEM electrolyzers, which is proportional to the volume generation rate. Therefore, controllers are given as

$$u_1 = k\dot{V}_1, \tag{27}$$

$$u_2 = k\dot{V}_2. \tag{28}$$

Using Eqs. 17-21, the final state space representation of the maneuverable device in twp degrees of freedom (DOF) including the defined controllers is given as

$$\begin{bmatrix} \dot{x_1} \\ \dot{x_2} \\ \dot{x_3} \\ \dot{x_4} \\ \dot{x_5} \\ \dot{x_6} \end{bmatrix} = \begin{bmatrix} x_2 \\ -\frac{c_x x_2}{M} + \frac{\rho g(V_0 + x_5 + x_6)}{M} - g \\ x_4 \\ \frac{c_\theta x_4}{I} + \frac{\rho g(\cos(x_5)L(x_5 - x_6) - \sin(x_5)H(x_5 + x_6))}{I} \\ 0 \\ 0 \end{bmatrix} + \begin{bmatrix} 0 & 0 \\ 0 & 0 \\ 0 & 0 \\ 0 & 0 \\ 1/k & 0 \\ 0 & 1/k \end{bmatrix} \begin{bmatrix} u_1 \\ u_2 \end{bmatrix}, \tag{29}$$

where x_1 is the depth, x_2 is the velocity in the vertical direction, x_3 is rotation, x_4 is the angular velocity, x_5 is the volume of balloons attached to the first BCD and x_6 is the volume of balloons attached to the second BCD.

The closed-loop control will be done using 2 PID controllers for 2 BCDs. The references are set differently to have a non-zero orientation. The relation between the depth references and the target depth and angle is determined by the geometry of the device.

$$r_1 = r - L\tan\theta, \tag{30}$$

$$r_2 = r + L\tan\theta, \tag{31}$$

where r is the depth of the target and θ is the angle of the target. K_P, K_I, and K_D, which can be found in Table II, are selected based on the automatic tuning based on the transfer function in Matlab Simulink. The control loop can be observed in Fig. 9. The simulation results for tracking fine depth and angle are observable in Fig. 10. Note that an additional disturbance force is added as a sinusoidal signal in both vertical and angular directions. The frequency of the disturbance is selected as 0.02 Hz and the amplitude is estimated as 20 times the average drag force applied to the device taken from previous simulations. Responses are stable and overshoots are not large enough to become significant, indicating that the selected controller parameters are convenient. The lengthy settling time is expected because of the slow gas generation/consumption rates of balloons and because of the lack of a less aggressive controller to provide a stable response both for the depth and the orientation.

The reason behind selecting a simpler control law instead of an advanced controller in this part is that the main interest

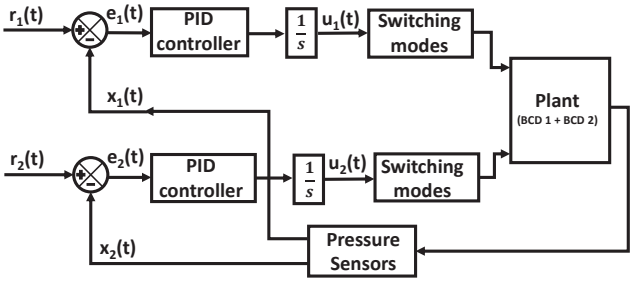

Fig. 9. Schematic of the orientation control.

of the study on the maneuverable device is demonstrating experimental validation of the concept of rotational motion with PEM Electrolyzers as actuators, apart from the study in the first part, which was also focused on improving the energy efficiency of hard actuators by using an advanced controller. In this part, the controller will be highly energy-efficient by itself because of having pure soft actuators without an addition of hard actuators.

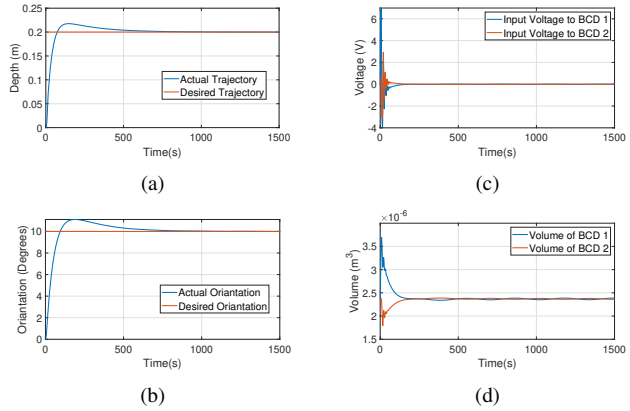

Fig. 10. Simulation results for fine depth and orientation control. (a) Desired and actual trajectory; (b) Desired and actual orientation; (c) Voltage for PEM electrolyzers; (d) Resultant volume of attached balloons.

TABLE II
CONTROL PARAMETERS

Parameter	Value	Parameter	Value
K_P	2.318	K_I	0.003
K_D	10.185	Q	1
R	0.3	M	1
P	5		

IV. EXPERIMENTAL VALIDATION

Two types of experiments have been carried out to validate this research. The first experiment was conducted to validate that using both thrusters and PEM electrolyzers achieves accurate and energy efficient depth control. The second experiment was conducted to validate that using PEM electrolyzers along can achieve noiseless and fine orientation control.

A. Experimental Setup

The control setup was composed of two power generators (KEPCO BOP 50-8D). One of those is for DC motors and the

other is for PEM electrolyzers. dSPACE (DS1104, dSPACE Inc.) was used to send the desired control signals (u_1 and u_2 in Fig. 7) to the power generators. An Arduino UNO was used to sense depth through the pressure sensor (SparkFun pressure sensor breakdown - MS5803-14BA). MATLAB Simulink 2017b was used for communication with Arduino and dSPACE, and for recording the data. The dSPACE is a convenient selection because of its robustness which prevents any latency or computation delays even for experiments that have small sampling times. The sampling time was 0.1 seconds in our experiment, which provides decent control performance. The experimental setup can be observed in Fig. 11. A buoyancy-enabled depth control device was designed using hard and soft actuators. A Blue Robotics Watertight Enclosure (SKU: WTE-VP) was used as a waterproof chamber that includes two PEM electrolyzers (Horizon, SKU: HFC-FCSU-023B), one water tank, and pipes for gas connections. The DC motors (LICHIFIT, ASIN:B07WY4MDYZ) were attached to the circumference of the chamber to apply thrust force. The reason for using two DC motors was to prevent the device from rotating. The pressure sensor (SparkFun, MS5803-14BA) was also attached to the circumference to observe the pressure and provide depth data. The dead weight was used to adjust the buoyancy of the device so that it became negative buoyant at the beginning of the experiment.

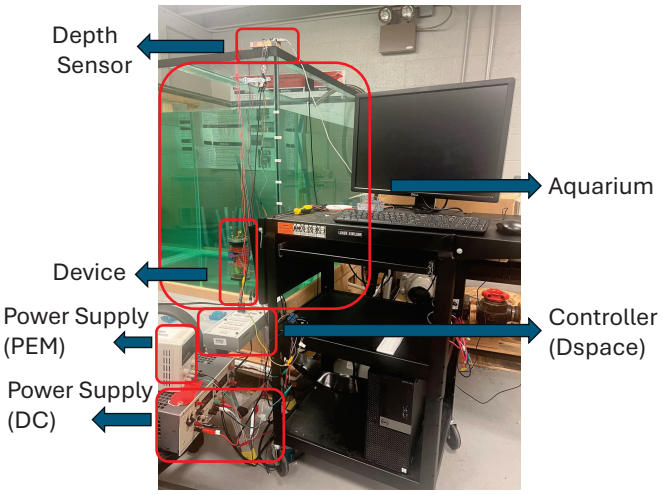

Fig. 11. Experimental setup.

B. Depth Control Results

Two different experiments have been conducted to make a clear comparison between the cases in which PEM electrolysis was used and those in which it was not, especially to observe the energy savings in the control input for DC motors. The corresponding result for the first case that the DC motor was used only can be found in Fig. 12, and the results when the PEM electrolysis was used in addition to the DC motors are shown in 13. According to the results, it is observed that there is an excessive amount of savings in the control energy when PEM is used. There are huge time intervals during which DC motors did not run at all because PEM electrolysis was able to keep the device at the desired level by bringing it to a neutrally buoyant level. According to estimates of energy consumption based on control input signals, it is observed that 72.94% of the control energy is saved when PEM electrolysis is used. Please note that the step changes in the reference were small. The linearized model around any equilibrium point is unstable. With a PID control, the dynamics of BCD can be stabilized [35]. However, due to the saturation of the controls: the gas generation and consumption rate, we have to program the reference sign with a sequence of small step changes in part [35].

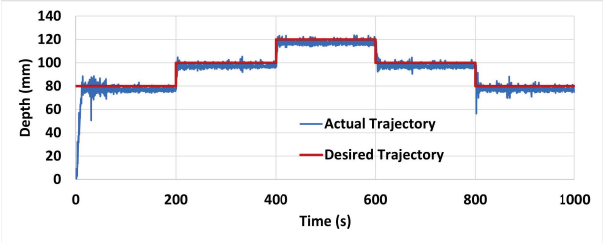

(a)

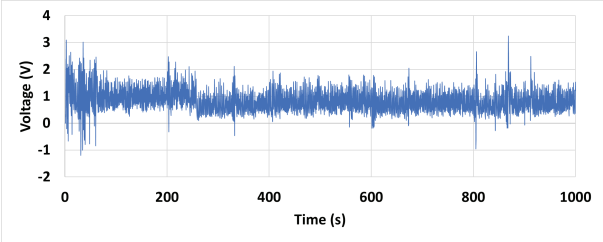

(b)

Fig. 12. Step reference tracking results when PEM electrolysis was not used. (a) Desired and actual trajectory; (b) Control input to the DC motors.

C. Orientation Control Results

The experimental setup for the depth and orientation control device includes two power generators, Dspace to send control signals to power generators, three Arduinos (two Arduino Nano and one Arduino UNO) to track the depth of two BCDs and to have serial communication with Dspace, and the experimental device. The overall setup can be observed in Fig. 11. The device was built up by basically attaching two BCDs that were defined in Section IV with a connector that was printed on a 3D printer. The application of non-homogeneous voltage inputs to two BCDs can provide oriented movement. The experiment was conducted to track a fine depth and angle. Since the maneuvering capacity of the device was not too large due to the limited volume of balloons, a small orientation angle (3.5 degrees) was tracked in the experiment along with a small value for depth tracking. The experimental results can be observed in Fig. 14.

In this experiment, a switching control was used to switch between the fuel cell mode and the electrolyzer mode based on the depth signal. Consequently, BCD #2 was in the gas generation mode, and BCD #1 was in the gas consumption mode throughout the experiment. Although gas generation was automatically adjusted by changes in the voltage input

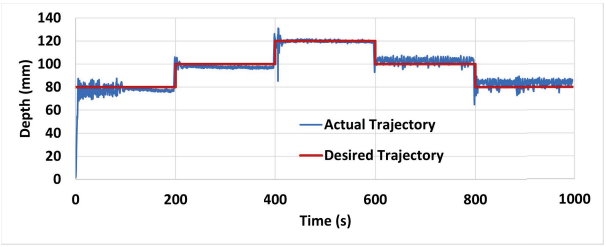

(a)

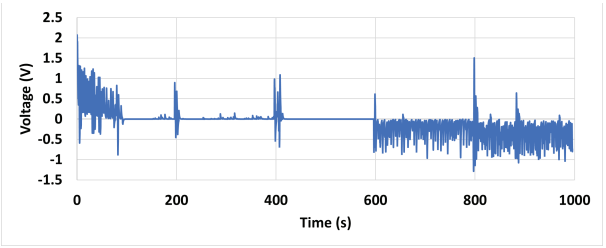

(b)

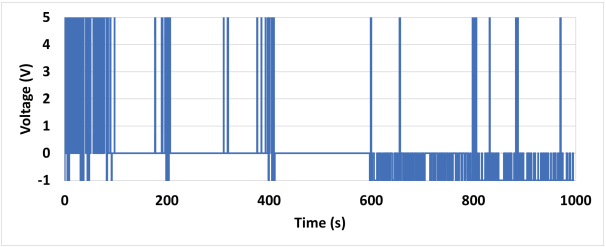

(c)

Fig. 13. Step reference tracking results when PEM electrolysis is used in combination with DC motors. (a) Desired and actual trajectory; (b) Control Input to the DC motors; (c) Control Input to the PEM electrolyzers.

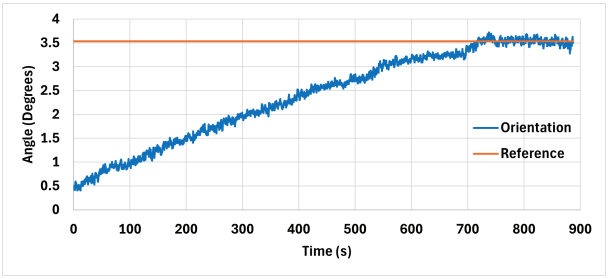

(a)

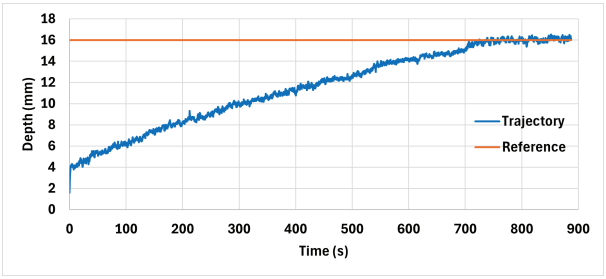

(b)

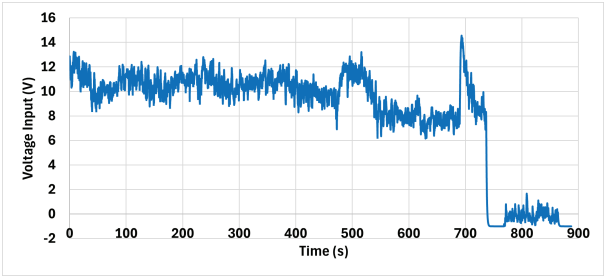

(c)

Fig. 14. Experimental results for fine depth and orientation control: (a) orientation angle; (b) depth; (c) voltage input to the BCD #2.

to the BCD #2, which can be observed in Fig. 14(c), gas consumption was kept at the maximum consumption capacity of the PEM cells throughout the experiment by connecting a resistor between two terminals of the BCD #2. That was done by the relay module, which provided automatic switching based on the signal from the controller. The results show that the novel design can track the fine depth (16 mm) and the fine angle (3.5 deg) without the use of hard actuators, and the device can maintain its final orientation and depth since PEM electrolysis provided a permanent buoyancy adjustment as shown in Fig. 14.

The results demonstrate that the usage of automatically controlled PEM electrolysis could be used for underwater vehicles to actuate in both vertical and rotational directions. The major difference of this method in comparison with existing methods of depth and orientation control is the energy efficiency due to providing a permanent change because of adjustment in buoyancy and the center of volume, instead of running hard actuators throughout the application to keep the position and orientation of the device at a desired level. The device will maintain its position even after the PEM electrolyzers are turned off, which prevents energy consumption.

V. Feasibility Study for Industrial Applications

In order to achieve larger and faster actuation, the real-time application can include a replacement with an industrial PEM electrolyzer that can provide a larger gas generation rate. For example, Titan EZ1000 can provide a production rate of 500 ml / min and 1000 ml / min for oxygen and hydrogen, respectively [36]. Those rates are 140 times higher than the educational product (Horizon educational PEM Fuel Cells) used in our work [37]. The weight of the product, 1.8 kg, makes it suitable for use in underwater devices.

The applicability of using PEM electrolyzers for BCDs requires consideration of larger weight changes during an underwater application and environments with higher pressures. In that manner, a possible solution for real-world application will be to use the latest industrial PEMs, which can produce gases much faster. In this paper, a case study is conducted in which an underwater device needs to grab a material from the ocean that has a weight of 5 kg at 3000 meters depth. The extra volume required to bring the device to a neutrally buoyant level would be 0.0048 m^3. Since hydrogen is expected to have a density of 20 kg/m^3 at 300 bars [38], the required amount of hydrogen to occupy the desired volume would be 0.096 kg.

Although production rates of up to 10 kgh^{-1} can be reached at 300 bars using PEM water electrolysis [39], while power consumption is 6.5 kW, a safer assumption will be made by taking the production rate as 1 kgh^{-1}, which is the hydrogen production rate of "Titan EZ1000". With this rate, the desired amount of hydrogen is produced in 346 seconds by spending

225 kJ.

The comparison between the cases of thrusters that use the addition of PEM electrolyzers with and without the addition of the PEM electrolyzers is estimated using the energy consumption data from our experiments. Since the extra weight that prevents the device from being natural buoyant is 5 kg instead of 20 g as in our experiment, the energy consumption rate is taken to be 250 times higher. The simulation is done for the time of the operations in a range of 1 to 4.6 hours. The corresponding energy savings by using PEM electrolysis can be observed in Fig. 15.

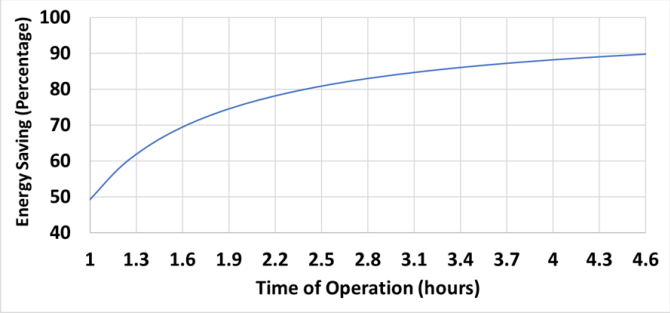

Fig. 15. The energy saving with respect to the time of operation at 300 bars.

As can be seen, PEM electrolyzers are still expected to save a significant amount of energy for underwater operations even though high pressure and larger change in weight are considered. Note that if higher pressure causes propellers to spend more energy, it would only help PEM electrolyzers to save larger percentages of energy.

VI. Conclusion and Future Work

In this article, we validate our previous studies on the usage of PEM electrolysis for the buoyancy and orientation control of AUVs through experimental tests. We designed two devices for this experiment. The first device is a buoyancy-enabled depth control device that integrates a combined thruster and a PEM electrolysis device, enabling vertical buoyancy control. We used MPC control for the thruster's DC motor and automatic switching control for PEM electrolysis. The results showed that the device successfully tracked depth while saving significant energy. The second device is an orientation and depth control device that exclusively uses PEM electrolysis as actuators. We used PID control for this device. This experimental study indicates that PEM electrolysis is an effective control method for underwater vehicles.

In this paper, we only used MPC control for the thruster and PID control for PEM to validate depth control. Comparison with other control strategies will be focused on in our future work. This study assumed steady water conditions without water currents and significant pressure changes. Although performance is expected to be steady even under a water current because of permanent changes in the buoyancy and volume center, future work can be followed by experimental validation under challenging conditions. Solutions to overcome possible challenges coming from disturbances of real applications can be listed as using industrial PEM electrolyzer to achieve fast and robust performance, using highly elastic, pressure-resistant, and chemically stable materials instead of regular plastic balloons such as neoprene rubber, silicon rubber, or Ethylene Propylene Diene Monomer (EPDM). Moreover, although the performance of PEM electrolyzers is expected to be the same or even more efficient [40], future work will focus on applications under higher pressure.

VII. Acknowledgment

Study concept, oversight, and funding were provided by the U.S. Department of the Interior, Bureau of Safety and Environmental Enforcement (BSEE), Office of Offshore Regulatory Program Branch, Sterling, VA under Contract Number 140E0123C0007. The content, statements, findings, opinions, conclusions, and recommendations are those of the author(s) and do not necessarily reflect the views of the Bureau of Safety and Environmental Enforcement.

References

[1] L. L. Whitcomb, "Underwater robotics: Out of the research laboratory and into the field," in *Proceedings 2000 ICRA. Millennium Conference. IEEE International Conference on Robotics and Automation. Symposia Proceedings (Cat. No. 00CH37065)*, vol. 1. IEEE, 2000, pp. 709–716.

[2] Z. Chen, T. I. Um, and H. Bart-Smith, "A novel fabrication of ionic polymer–metal composite membrane actuator capable of 3-dimensional kinematic motions," *Sensors and Actuators A: Physical*, vol. 168, no. 1, pp. 131–139, 2011.

[3] L. J. Hamdan, J. L. Salerno, A. Reed, S. B. Joye, and M. Damour, "The impact of the deepwater horizon blowout on historic shipwreck-associated sediment microbiomes in the northern gulf of mexico," *Scientific reports*, vol. 8, no. 1, pp. 1–14, 2018.

[4] B. K. Tiwari and R. Sharma, "Design and analysis of a variable buoyancy system for efficient hovering control of underwater vehicles with state feedback controller," *Journal of Marine Science and Engineering*, vol. 8, no. 4, p. 263, 2020.

[5] C. Yue, S. Guo, and L. Shi, "Hydrodynamic analysis of the spherical underwater robot SUR-II," *International Journal of Advanced Robotic Systems*, vol. 10, no. 5, p. 247, 2013.

[6] H. Kang, "The study of DC motor noise and vibration," *SAE transactions*, pp. 2461–2467, 1995.

[7] W. Kirkwood and D. Steele, "Active variable buoyancy control system for MBARI's ROV," in *Proceedings of OCEANS'94*, vol. 2. IEEE, 1994, pp. II–471.

[8] S. Tangirala and J. Dzielski, "A variable buoyancy control system for a large AUV," *IEEE Journal of Oceanic Engineering*, vol. 32, no. 4, pp. 762–771, 2007.

[9] S. D. Lim, A. P. Mazzoleni, J.-k. Park, P. I. Ro, and B. Quinlan, "Conceptual design of ocean compressed air energy storage system," *Marine Technology Society Journal*, vol. 47, no. 2, pp. 70–81, 2013.

[10] A. Keow, Z. Chen, and H. Bart-Smith, "PIDA control of buoyancy device enabled by water electrolysis," *IEEE/ASME Transactions on Mechatronics*, vol. 25, no. 3, pp. 1202–1210, 2020.

[11] H. Samadi-Boroujeni, A. Altaee, H. Khabbaz, and J. Zhou, "Application of buoyancy-power generator for compressed air energy storage using a fluid–air displacement system," *Journal of Energy Storage*, vol. 26, p. 100926, 2019.

[12] T. Love, D. Toal, and C. Flanagan, "Buoyancy control for an autonomous underwater vehicle," *IFAC Proceedings Volumes*, vol. 36, no. 4, pp. 199–204, 2003.

[13] M. Choyekh, N. Kato, R. Dewantara, H. Senga, and H. Chiba, "Depth and altitude control of an AUV using buoyancy control device," *Journal of Electrical Engineering*, vol. 4, pp. 133–149, 2016.

[14] Y. Wang, D. F. R. Diaz, K. S. Chen, Z. Wang, and X. C. Adroher, "Materials, technological status, and fundamentals of PEM fuel cells–a review," *Materials today*, vol. 32, pp. 178–203, 2020.

[15] M. Carmo, D. L. Fritz, J. Mergel, and D. Stolten, "A comprehensive review on PEM water electrolysis," *International journal of hydrogen energy*, vol. 38, no. 12, pp. 4901–4934, 2013.

[16] J. Yazji, A. Keow, H. Zaidi, L. T. Torres, C. Leroy, and Z. Chen, "Buoyancy control device enabled by reversible proton exchange membrane fuel cells for fine depth control," *Journal of Dynamic Systems, Measurement, and Control*, vol. 143, no. 3, 2021.
[17] A. Keow and Z. Chen, "Auto-tuning control of proton exchange membrane water electrolyzer with self-assessment and gain scheduling," *Journal of Dynamic Systems, Measurement, and Control*, vol. 143, no. 5, 2021.
[18] A. Keow, W. Zuo, F. Ghorbel, and Z. Chen, "Reversible fuel cell enabled underwater buoyancy control," *Mechatronics*, vol. 86, p. 102865, 2022.
[19] C. Zavislak, A. Keow, Z. Chen, and F. Ghorbel, "Auv buoyancy control with hard and soft actuators," *IEEE Control Systems Letters*, vol. 5, no. 6, pp. 1874–1879, 2020.
[20] ——, "AUV tool manipulation with hard and soft actuators," *IEEE Robotics and Automation Letters*, vol. 6, no. 4, pp. 8553–8560, 2021.
[21] A. Keow, W. Zuo, F. Ghorbel, and Z. Chen, "Underwater buoyancy and depth control using reversible PEM fuel cells," in *2020 IEEE/ASME International Conference on Advanced Intelligent Mechatronics (AIM)*. IEEE, 2020, pp. 54–59.
[22] W. Zuo, X. Yi, F. H. Ghorbel, and Z. Chen, "Optimal trajectory planning and control of buoyancy control device enabled by water electrolyzer," in *2019 IEEE 58th Conference on Decision and Control*. IEEE, 2019, pp. 2120–2125.
[23] D. Koc, W. Zuo, F. Ghorbel, and Z. Chen, "Energy efficient depth control for underwater devices using soft and hard actuators," in *2023 IEEE/ASME International Conference on Advanced Intelligent Mechatronics (AIM)*. IEEE, 2023, pp. 916–921.
[24] T. Kaaya, W. Zuo, F. Ghorbel, and Z. Chen, "Dynamics and control of auvs using buoyancy-induced soft actuation enabled by reversible fuel cells," *Journal of Dynamic Systems, Measurement, and Control*, 2025, under review.
[25] C. Hoppe, F. Ghorbel, and Z. Chen, "Dynamics and control of AUVs using buoyancy-based soft actuation," in *2023 American Control Conference*. IEEE, 2023, pp. 4543–4548.
[26] S. A. Grigoriev, V. N. Fateev, H. Middleton, T. O. Saetre, and P. Millet, "A comparative evaluation of palladium and platinum nanoparticles as catalysts in proton exchange membrane electrochemical cells," *International Journal of Nuclear Hydrogen Production and Applications*, vol. 1, no. 4, pp. 343–354, 2008.
[27] A. ElGhazali and S. Dol, "Aerodynamic optimization of unmanned aerial vehicle through propeller improvements," *Journal of Applied Fluid Mechanics*, vol. 13, no. 3, pp. 793–803, 2020.
[28] E. F. Camacho and C. B. Alba, *Model predictive control*. Springer science & business media, 2013.
[29] D. Q. Mayne, E. C. Kerrigan, and P. Falugi, "Robust model predictive control: advantages and disadvantages of tube-based methods," *IFAC Proceedings Volumes*, vol. 44, no. 1, pp. 191–196, 2011.
[30] D. E. Seborg, T. F. Edgar, D. A. Mellichamp, and F. J. Doyle III, *Process dynamics and control*. John Wiley & Sons, 2016.
[31] S. Vazquez, J. Rodriguez, M. Rivera, L. G. Franquelo, and M. Norambuena, "Model predictive control for power converters and drives: Advances and trends," *IEEE Transactions on Industrial Electronics*, vol. 64, no. 2, pp. 935–947, 2016.
[32] K. Holkar and L. M. Waghmare, "An overview of model predictive control," *International Journal of control and automation*, vol. 3, no. 4, pp. 47–63, 2010.
[33] J. Rodriguez, M. P. Kazmierkowski, J. R. Espinoza, P. Zanchetta, H. Abu-Rub, H. A. Young, and C. A. Rojas, "State of the art of finite control set model predictive control in power electronics," *IEEE Transactions on Industrial Informatics*, vol. 9, no. 2, pp. 1003–1016, 2012.
[34] I. Olkin, "Jacobians of matrix transformations and functions of matrix argument," *Journal of the American Statistical Association*, vol. 94, no. 446, pp. 652–653, 1999.
[35] Z. Chen, T. I. Um, and H. Bart-Smith, "Modeling and control of artificial bladder enabled by ionic polymer-metal composite," in *2012 American Control Conference (ACC)*. IEEE, 2012, pp. 1925–1930.
[36] *Titan Series Technical Data Sheet*, Fuel Cell Store, College Station, Texas, USA, technical specifications for PEM electrolyzer cell stack. [Online]. Available: https://www.fuelcellstore.com/pem-electrolyzer-cell-stack-titan-1000
[37] *FCSU-023 User Manual*, Horizon Educational, product Reference No.: FCSU-023-1. [Online]. Available: https://www.horizoneducational.com/pem-blue-reversible-fuel-cell-1-unit/p1239
[38] S. Makridis, "Hydrogen storage and compression," *arXiv preprint arXiv:1702.06015*, 2017.
[39] R. Hancke, T. Holm, and Ø. Ulleberg, "The case for high-pressure PEM water electrolysis," *Energy Conversion and Management*, vol. 261, p. 115642, 2022.
[40] F. Marangio, M. Santarelli, and M. Calì, "Theoretical model and experimental analysis of a high pressure PEM water electrolyser for hydrogen production," *International journal of hydrogen energy*, vol. 34, no. 3, pp. 1143–1158, 2009.

Denizcan Koc is a PhD candidate in the Mechanical Engineering Department at the University of Houston. Deniz was born in Ankara/Turkey in 1997. He received his BS degree in Mechanical Engineering at the Middle East Technical University in 2021. He joined to Buoyancy-inspired Robotics Control Lab in Januray, 2022. His current research is focused on soft robotics including underwater buoyancy control and actuation by Proton Exchange Membrane (PEM) electrolysis.

Qiang Zhu is a PhD student in the Mechanical Engineering Department at the University of Houston. He received his bachelor degree in Packaging Engineering at Jilin University in 2018. Then he got the master degree in Mechanical Engineering at the George Washington University in 2020. His research interests focus on navigation and control of underwater robots.

Fathi H. Ghorbel received the B.S. degree with honors from the Pennsylvania State University, Philadelphia, the M.S. degree from Carnegie-Mellon University, Pittsburgh, PA, and the Ph.D. degree from the University of Illinois at Urbana-Champaign, in 1985, 1987, and 1991, respectively, all in mechanical engineering.,He is a Professor in the Department of Mechanical Engineering and Materials Science, Rice University, Houston, TX, where he serves as the Director of Graduate Studies. He has a joint appointment in the Department of Bioengineering. He is the Director of the Robotics and Intelligent Systems (RiSYS) Laboratory. His research is in the areas of dynamic systems and control, robotics, and biomedical engineering systems. Dr. Ghorbel is a Member of the ASME, a member of Sigma Xi, IFAC, SIAM, lASTED, and ASEE.

Zheng Chen was born in Hengyang, China. He received the B.E. degree in electrical engineering and the M.E. degree in control science and engineering from Zhejiang University, Hangzhou, China, in 1999 and 2002, respectively, and the Ph.D. degree in electrical engineering from Michigan State University, East Lansing, MI, USA, in 2009. He was a Research Associate with the University of Virginia, Charlottesville, VA, USA, from 2009 to 2012, a Research and Development Engineer specializing in control systems with Baker Hughes from 2012 to 2013, and an Assistant Professor of electrical engineering and computer science with Wichita State University, Wichita, KS, USA, from 2013 to 2017. He is currently an Associate Professor of mechanical engineering with the University of Houston, Houston, TX, USA. His current research interests include dynamic systems and control, smart material sensors and actuators, and bio-inspired underwater robots.